CrossMark

ORIGINAL ARTICLE

Optical, in situ, three-dimensional, absolute shape measurements in CNC metal working lathes

R. Kuschmierz[1] · A. Davids[2] · S. Metschke[3] · F. Löffler[3] · H. Bosse[3] · J. Czarske[1] · A. Fischer[1]

Abstract Temperature drifts, tool deterioration, unknown vibrations, as well as spindle play are major effects which decrease the achievable precision of CNC lathes and lead to shape deviations of the processed workpieces. Since currently no measurement system exists for precise, in situ, 3D shape monitoring, much effort is required to simulate and compensate these effects. In this article, we propose an optical measurement principle for first part quality manufacturing. The absolute shape, meaning the diameter and surface profile, of the workpiece is determined from its tangential velocity and the surface distance. In order to allow keyhole access, both measurands are determined simultaneously with a single sensor. Measurements inside a metal working lathe show that the standard uncertainty for the absolute shape measurement is below 1 μm. The measurement uncertainty is nearly independent of the lateral surface velocity and roughness. The in situ measurements are compared to measurements with a tactile coordinate measurement machine for reference.

Keywords Lathe monitoring · Absolute shape · Optical measurement · In situ measurement

✉ R. Kuschmierz
  robert.kuschmierz@tu-dresden.de

1 Laboratory for Measurement and Sensor SystemTechniques, Technische Universität Dresden, Dresden, Germany

2 Institute of Manufacturing Technology, Technische Universität Dresden, Dresden, Germany

3 Division 5 Precision Engineering, Physikalisch-Technische Bundesanstalt, Braunschweig, Germany

1 Introduction

1.1 State-of-the-art

The achievable precision of computerized numerically controlled (CNC) lathes is currently limited by temperature drifts, tool wear, spindle vibration, and axle play [1–3]. These disturbances can be compensated in part, for instance by employing temperature compensation and a compensation of tool wear by respective measurements or predictions [4–10]. However, in order to guarantee deviations from the desired shape below 1 μm, shape measurements are still required.

The most versatile and precise tool for this purpose is a tactile coordinate measurement machine (CMM), which can be regarded as a gold standard. However, the testing with a CMM is very slow compared to the production time, because it is not performed in situ, but in separate machines meaning the specimen has to be reclamped. Furthermore, the probing process itself is time consuming due to its tactile nature and for avoiding scratches on the surface of the specimen. Thus, only few samples can be measured with a CMM. By conducting tactile measurement inside the lathe [11], the possible sample size can be increased, but the required measurement time still exceeds the production time.

Non-contact measurement techniques such as optical techniques offer higher measurement rates and could therefore allow a hundred percent process monitoring, which is necessary for first part quality manufacturing. Shadow projection for instance can scan the absolute three-dimensional shape of a shaft in just a few seconds [12] and was already successfully applied in a metal working lathe. However, it is unable to resolve concave profiles and too bulky to easily fit into a lathe, since sending and detection unit of the system are on opposite sides of the specimen.

Thus, optical techniques with keyhole access are required, such as triangulation, chromatic confocal sensing, absolute distance interferometry, or fringe projection [13–16]. All of these techniques can achieve sub-micron precision as well as sufficiently high measurement rates of several kHz for surface profile measurements at stationary and smooth objects. Some of these techniques have already been employed at non moving objects for close to machine measurements [17] and even for in situ measurements [18].

However, all of these techniques suffer from the speckle effect, especially at moving rough surfaces which increases the achievable measurement uncertainty. Furthermore, none of these techniques is able to measure the absolute shape, i.e., the angle resolved radius of the workpiece, since exact knowledge of the distance from the sensor to the rotational axis is necessary additionally to the measured distance between sensor and surface. Otherwise, tumbling, vibrations, eccentricity, and drifts of the rotational axis-sensor distance lead to measurement errors.

The measurement errors can be avoided by using multiple optical distance sensors around the specimen [19, 20]. This requires multiple optical accesses, however. As an alternative with keyhole access capability, the laser Doppler distance sensor with phase evaluation (P-LDD sensor) can be employed. The P-LDD sensor offers a lateral velocity measurement in addition to the axial distance measurement [21–24]. This enables the simultaneous measurement of the mean radius and the deviation from the mean radius of the rotating workpiece. As a result, an absolute shape measurement with a single sensor is possible. While the P-LDD sensor principle has been tested successfully in the laboratory, its applicability for fast and precise, 3D shape monitoring in situ in CNC lathes has to be investigated.

1.2 Aim and outline of the paper

The aim of this paper is to apply a P-LDD sensor for in situ, three-dimensional (3D), absolute shape measurements in a CNC lathe and to characterize the achievable measurement uncertainty. The measurement approach is based on

a simultaneous measurement of the distance of the surface as well as the tangential velocity of the specimen with a single sensor, which is described in Section 2. The principle and setup of the P-LDD sensor, which is capable to perform these simultaneous measurements, is subsequently explained in Section 3. In order to fit the sensor into the lathe, it was miniaturized for the first time. Experimental results regarding the influence of the micro and macro geometry of the workpiece toward the achievable measurement uncertainty are presented in Section 4. Finally, the absolute three-dimensional shape measurement in a CNC lathe is presented in Section 5, thereby validating and characterizing the capabilities of the P-LDD sensor system.

2 Approach for absolute shape measurement with keyhole access

The absolute 3D shape of a workpiece can be described by its radius $r(\alpha, \tilde{z})$ in cylindrical coordinates, with the rotation angle α and the height $\tilde{z}$, cf. Fig. 1. An indirect measurement of the shape has to be performed, because it is not possible to measure the radius directly with keyhole access. For this purpose, the shape is described as

$$r(\alpha, \tilde{z}) = R + \Delta r(\alpha, \tilde{z}), \tag{1}$$

with the radius of the Gaussian cylinder

$$R = \frac{1}{(2\pi \cdot l)} \int_0^{2\pi} \int_0^l r(\alpha, \tilde{z}) \, d\tilde{z} \, d\alpha, \tag{2}$$

subsequently named mean radius and the deviations $\Delta r(\alpha, \tilde{z})$ from R. As a result, the shape measurement can be accomplished by measuring the mean radius R and the radius deviations $\Delta r(\alpha, \tilde{z})$.

For measurements of $\Delta r(\alpha, \tilde{z})$, subsequently named surface profile, optical distance sensors are well equipped, since they offer distance uncertainties below 1 μm. The output of the distance sensor is the distance z between the sensor and the surface of the object, cf. Fig. 1. When the distance measurement is continuously performed during the

Fig. 1 Schematic of measurement principle. The tangential velocity v and the surface distance z of the rotating workpiece are measured simultaneously and result in the angular resolved radius $r(\alpha)$. Feeding the sensor along the $\tilde{z}$-axis enables a 3D shape measurement with keyhole access. Note that the machine coordinates are denoted by the tilde sign
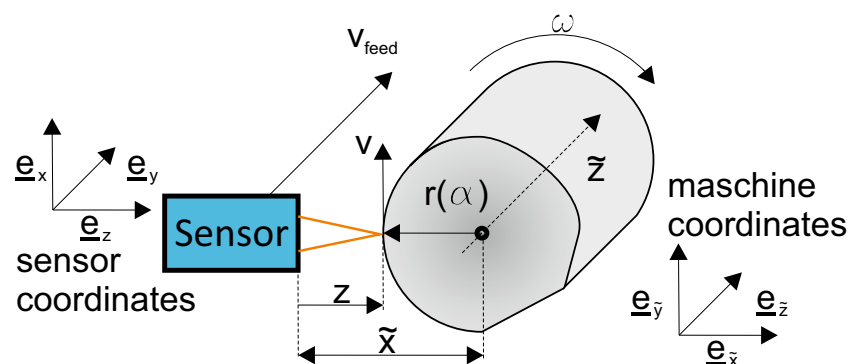
rotation of the object, the surface profile results from n distance measurements to

$$\Delta r(\alpha, \tilde{z}) = Z - z(\alpha, \tilde{z}) = -\Delta z \qquad (3)$$

with $Z = \frac{1}{n} \sum_{i=1}^{n} z(\alpha, \tilde{z})$, under the assumption of negligible eccentricity of the workpiece in respect to the rotational axis. For absolute shape measurements, the sole measurement of $\Delta r(\alpha, \tilde{z})$ requires a known distance $\tilde{x}$ between sensor and rotational axis, cf. Fig. 1. Otherwise, any uncertainty in the alignment between sensor and rotational axis, for instance due to thermal drifts, directly increases the uncertainty of the mean radius measurement.

Therefore, a novel approach for the absolute shape measurement is proposed, which does not require the distance $\tilde{x}$ to be known. By measuring the tangential surface velocity $v(\alpha, \tilde{z})$, R results to

$$R = \frac{V}{\omega} \qquad (4)$$

with $V = \frac{1}{n} \sum_{i=1}^{n} v(\alpha, \tilde{z})$. Employing a simultaneous measurement of the lateral velocity v and the axial position z the shape measurement is thus obtained according to the Eqs. 1, 3, 4 by

$$r(\alpha, \tilde{z}) = \frac{V}{\omega} - \Delta z(\alpha, \tilde{z}). \qquad (5)$$

As a result, the novel approach for the shape measurement is independent of sensor and axle misalignment in $\tilde{x}$-direction. Note that this approach requires the angular velocity of the workpiece to be known (which is the case for CNC lathes, typically), in order to calculate R. Furthermore, $\tilde{z}$ has to be known, to calculate the 3D shape.

3 Sensor principle and setup

3.1 Sensor principle

The measurement principle of the laser Doppler distance sensor with phase evaluation (P-LDD sensor) allows for the simultaneous measurement of lateral velocity and position of moving and optically rough surfaces. The measurement principle of the P-LDD sensor is based on laser surface velocimetry (LSV) [25]. An LSV uses an interference fringe pattern formed in the intersection of two coherent laser beams and measures the velocity component perpendicular to the fringe system. In order to calculate the velocity, the measured Doppler frequency of the scattered light signal of an object f_D and the calibrated fringe spacing d are evaluated by

$$v = f_D \cdot d(z). \qquad (6)$$

Due to aberrations and slightly distorted wave fronts, the fringe spacing is not constant along the measurement volume. This effect restricts the relative velocity measurement uncertainty of a LSV fundamentally to 0.1 % < $\sigma_v/v < 1$ % [26], because the surface position and accordingly the exact fringe spacing are unknown. The P-LDD sensor overcomes this limitation by superposing two mutually tilted interference fringe patterns and evaluating the two scattered light signals, which allows for an additional position measurement [21]. The fringe systems exhibit a position dependent, mutual phase shift, which leads to a phase difference φ in the scattered light signals

$$\varphi(z) = z \cdot s(z) \qquad (7)$$

with the slope

$$s(z) = 2\pi \frac{2 \tan \Psi/2 \cos \Psi/2}{d(z)} \approx 2\pi \frac{\tan \Psi}{d(z)} \qquad (8)$$

of the phase shift depending on the tilting angle ψ between the fringe patterns. Thus, evaluating the phase shift $\varphi(z)$ in addition to the Doppler frequencies allows for a distance measurement simultaneous to the velocity measurement. Furthermore, the velocity measurement uncertainty is decreased, because it is not limited by the fringe spacing uncertainty anymore. Note that the approximation in Eq. 8 is valid only for small tilting angles. Furthermore, the tilt of the fringe systems with respect to the measurement axis has to be considered for the velocity measurement perpendicular to the measurement axis. In Fig. 2, the tilted fringe patterns and the resulting scattered light signals are depicted schematically.

An error propagation of Eq. 7 shows, that in order to achieve a low distance uncertainty $\sigma_z = s(z)^{-1} \cdot \sigma_\varphi$, a steep slope $s(z)$ of the calibration function is required. However, the phase evaluation leads to an ambiguous calibration function $\varphi(z)$, because the unambiguous phase range is limited to $-\pi \le \varphi(z) < \pi$. Hence, the required steep calibration function hinders a large measurement range for the distance measurement. In order to increase the measurement range, a third fringe system with a slightly different tilting angle is superposed, which results in an additional, unambiguous calibration function to resolve the ambiguity issue [27]. In Fig. 3, the three fringe patterns and the resulting calibration functions $\varphi_{12}(z)$, $\varphi_{31}(z)$ are depicted schematically.

3.2 Sensor setup

In order to be able to fit the sensor into a lathe, a compact design was developed. By using fiber-coupled laser diodes and photo detectors, the sensor head (size $10 \times 10 \times 5$ cm^3) was realized in an all passive manner. Furthermore, the sensor head uses Invar as base plate material, in order to reduce the thermal elongations and misalignment of the optical components. The three laser diodes are temperature stabilized, to reduce thermal wavelength drifts as well. The laser
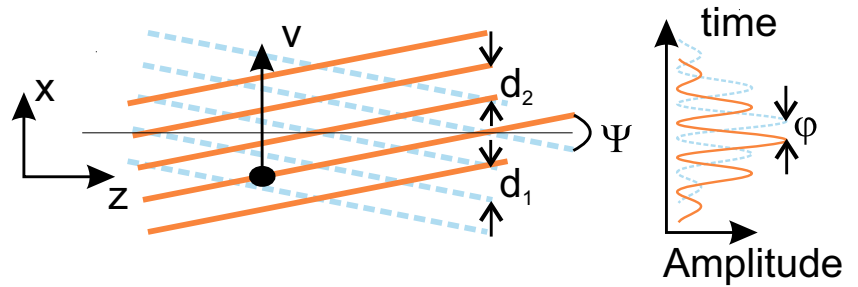
light with the wavelengths $\lambda_1 = 638$ nm, $\lambda_2 = 658$ nm, and $\lambda_3 = 685$ nm is coupled into one single mode fiber. The trichromatic light is collimated and split spatially by a blazed transmission diffraction grating, with the grating constant $g = 4$ µm. A narrow band stop filter (NF) then blocks the $+1$. diffraction order (DO) from λ_2 and a narrow band pass filter (BP) blocks the -1. DO from λ_1 and λ_3. The remaining ± 1. and 0. DO are superposed by a Keplerian telescope ($f_1 = f_2 = 40$ mm). As a result, three interference fringe systems with $d \approx 4$ µm, a lateral diameter $2 \cdot w_0 \approx 50$ µm, and an axial dimension $l_z \approx 600$ µm are formed in the intersection of the laser beams, cf. Fig. 3.

The tilt $\Psi_{12} \approx 9.32°$ between the fringe systems with the wavelengths λ_1, λ_2 results from superposing different diffraction orders, whereas $\Psi_{31} \approx 0.35°$ is due to the slight wavelength difference between λ_3 and λ_1. As a result, a steep calibration function with the slope $s_{12}(z) \approx 15°/$µm and and unambiguous calibration function with the slope $s_{31}(z) \approx 0.55°/$µm are formed (Fig. 4).

The scattered light is forwarded by two mirrors (M_1, M_2) and through the respective filters. As a result, the light with

the wavelength λ_2 is focussed into the upper multimode fiber A. The scattered light with the wavelengths λ_1 and λ_3 is focussed into the lower multimode fiber B and divided by wavelength in a separate fiber coupled unit. Three fiber coupled avalanche photo diodes are employed to detect the three scattered light signals.

The electronic output signals of the detectors are finally digitized using a digitizer board and analyzed on a computer using MATLAB. The Doppler frequencies are calculated using the discrete Fourier transformation and the phase difference using the cross-correlation function from the time series of the aquired signals. The velocity and distance are then calculated employing the calibration functions Eqs. 6, 7.

In order to calculate the Doppler frequency f_D and phase difference φ, a time series has to be recorded and analyzed. During the length of this time series, the surface is moving. Therefore, the lateral resolution in the direction of the movement will decrease. Since the standard uncertainty of the Doppler frequency depends on the length of the observed surface [28], time series from constant surface lengths of 1 mm are analyzed. For this purpose, the length of the time series is calculated from the estimated circumferential surface velocity using a priori knowledge of the workpiece velocity and the sampling frequency of the digitizer board. This ensures a constant uncertainty. Thus, a constant lateral resolution along the circumference of 1 mm is achieved, while the lateral resolution along the height remains 50 µm, due to the lateral diameter of the measurement volume.
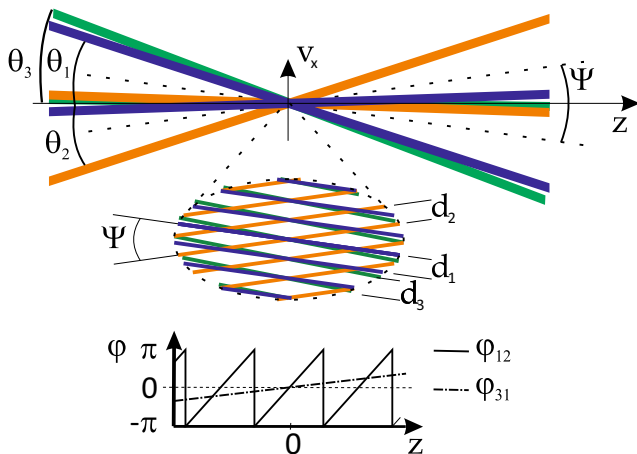

Fig. 3 Three mutually tilted interference fringe systems of a P-LDDS (*top*), and resulting calibration functions. The unambiguous calibration function φ_{31}, which results from the fringe systems 3 and 1, offers an absolute distance measurement with higher distance uncertainty, while the steep calibration function φ_{12}, which results from the fringe systems 1 and 2, offers a low distance uncertainty

4 Experimental setup and results

4.1 Experimental setup

In order to characterize the sensor performance and capabilities with respect to in situ lathe monitoring, experiments were performed in two different CNC lathes, in an Index G200 as well as in a CD402. For testing, shafts with different roughness, shapes, and diameters were manufactured and the shape of the resulting workpiece was measured with

Fig. 4 All passive, interferometric sensor head. The trichromatic light is introduced via the sending fiber. Grating and Keplerian telescope generate the three fringe systems. The mirrors M_1, M_2 forward the scattered light into the detection fibers
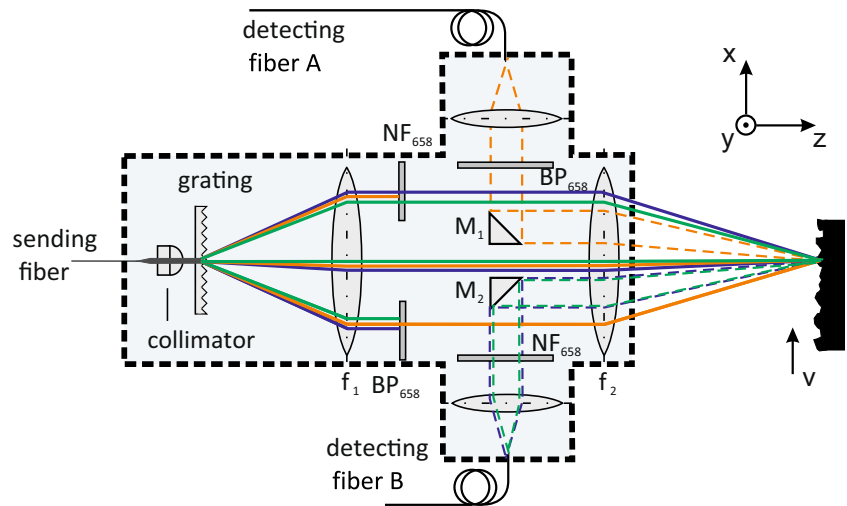
the P-LDD sensor. For reference measurements, a tactile coordinate measurement machine ULM 600 was employed.

In the Index G200, the P-LDD sensor is mounted onto the tool revolver, see Fig. 5 (top). This allows to position, the sensor freely using the same program employed for the specimen manufacturing. In the CD402 the sensor is
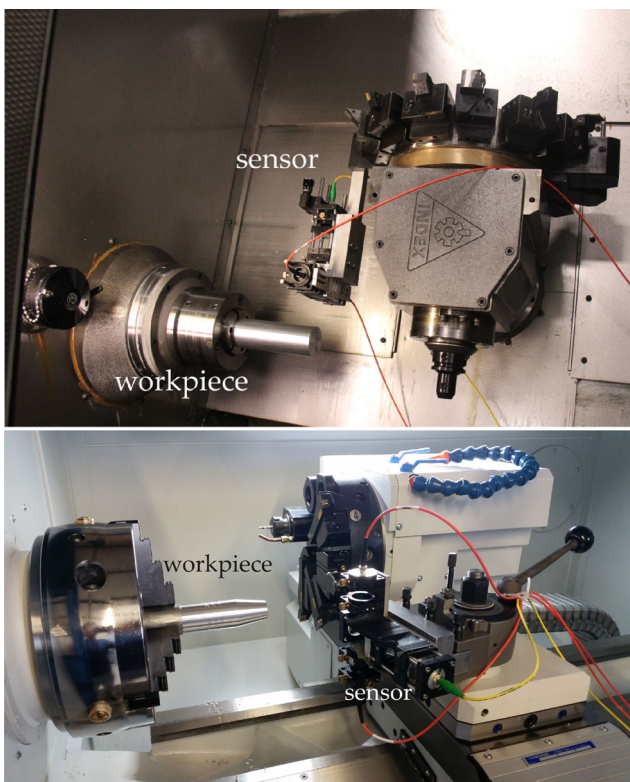

Fig. 5 Sensor mounted in different lathes. *Top*: the sensor head is mounted onto the tool revolver, which allows for a free positioning. *Bottom*: the sensor head is mounted opposite of the tool revolver, so that simultaneous cutting and measuring are possible in principle. The optical fibers for sending and receiving are fed through the chippings conveyor

mounted on a tool holder opposite of the tool revolver, cf. Fig. 5 (bottom). This allows for an in-process monitoring in principle, since cutting and sensing can be performed simultaneously from opposite sides. In this first test, the sensor is detached during manufacturing in order to protect the sensor from chippings, lubricants, and coolants. After reattaching the sensor, it is calibrated, in order to compensate for possible misalignment of the optical components. During the measurement, the spindle is rotating with 25 and 30 Hz, respectively. For scanning, the feed velocity is set to 36 to 1000 mm/min.

4.2 Measurement uncertainty

4.2.1 Theoretical measurement uncertainty

Due to the high number of measurements with the P-LDD sensor (10 workpieces with over 100,000 measurement points each), a complete comparison with the measurements from a CMM is not feasible. Instead, first the standard deviation for the radius measurements σ_r is calculated from the relative standard deviations for the velocity measurement σ_v/v and the standard deviations for the distance measurement σ_z. For this purpose, any noise or deviation in the measured distances or velocities are regarded as measurement uncertainties. This means that the workpieces under test are assumed to be perfectly shaped. An error propagation of Eq. 5 then yields

$$\sigma_r = \sqrt{\sigma_R^2 + \frac{\sigma_z^2}{M}}, \text{ with } \sigma_R = \frac{\sigma_v}{v}\frac{R}{\sqrt{N}} \qquad (9)$$

and with the total number of measurements N and the number of repeating measurements of the same surface segment M. For a scanning measurement with constant feed velocity, no surface segment is measured more then once ($M = 1$). Thus, σ_z cannot be reduced by averaging. It can be seen that

Fig. 6 Standard deviation of position and velocity in dependency of the surface roughness R_a and material
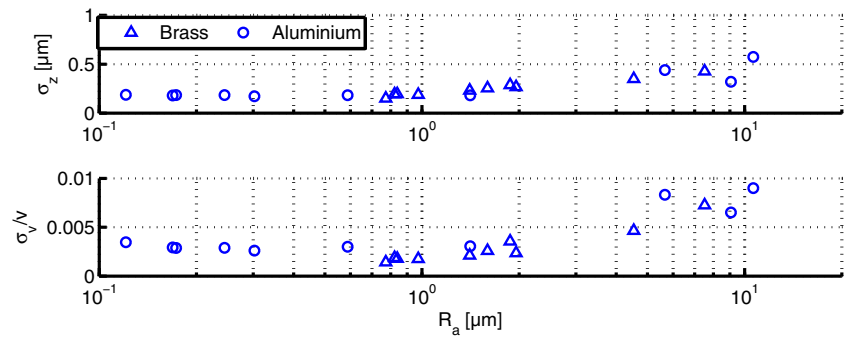
σ_z directly increases σ_r, cf. Eq. 9. Furthermore, it can be seen that σ_R increases with increasing R and σ_v/v and can be reduced by averaging. In order to quantify the measurement uncertainty, the influence of the micro geometry and the shape of the object are investigated next.

4.2.2 Micro geometry

Since the measurement with the P-LDD sensor depends on the speckle effect [29], the influence of the surface roughness toward the measurement uncertainty is investigated first. For this purpose, cylindrical probes with different roughness profiles are manufactured, by using different materials and by varying the feed velocities v_{feed} between 2 and 2000 mm/min during production. This leads to an average roughness 100 nm $\leq R_a \leq$ 10 µm.

In Fig. 6, the standard deviation σ_z for the position measurement and the relative standard deviation σ_v/v of the velocity measurement in dependency of the surface roughness R_a are shown. Standard deviations of $\sigma_z \approx$ 200 nm and $\sigma_v/v \approx$ 0.3 % are achieved for 100 nm < R_a < 1 µm. While the signal-to-noise-ratio (SNR) increases slightly (from 3 to 10 dB), due to an increase of the back scattered light at rough surfaces, both deviations also increase slightly for R_a > 1 µm. This increase in the standard deviations is assumed to be caused by increasing deviations of the shape

of the workpiece. Regarding the standard uncertainty of the shape, with $R =$ 20 mm and $N =$ 100,000, $\sigma_r \approx$ 300 nm results for R_a < 1 µm increasing to $\sigma_r \approx$ 700 nm for $R_a =$ 10 µm, cf. Eq. 9. Thus, the requirement for shape uncertainties below 1 µm is fulfilled even at rough surfaces.

Note that the different material (brass and aluminum) have no influence toward the measurement uncertainty. Note also that the measurements were performed with feed the velocity 1 mm/s (depicted in Fig. 6) and 17 mm/s, but that the feed velocity shows no influence toward σ_v/v and σ_z. Hence, the sensor performs well on optically rough surfaces in contrast to conventional laser optical distance sensors and is well suited for different materials and allows high scanning speeds.

4.2.3 Macro geometry

The influence of the surface macro geometry is investigated regarding two important aspects. Firstly, optical distance sensors are known to have difficulties measuring tilted surfaces. Secondly, the shape uncertainty is influenced by the diameter of the work piece, cf. Eq. 9. Thus, the influence of a surface tilt as well as the mean diameter of the surface is investigated.

In order to investigate the influence of tilted surfaces, a specimen with a varying cone angle $\gamma = \arctan(dR/d\tilde{z})$ is

Fig. 7 Specimen with varying cone angle γ. The sensor is moved with a constant distance to the surface of the workpiece and measures perpendicularly to the rotational axis, resulting in a tilt γ between the sensor axis $\underline{e}_z$ and the surface normal
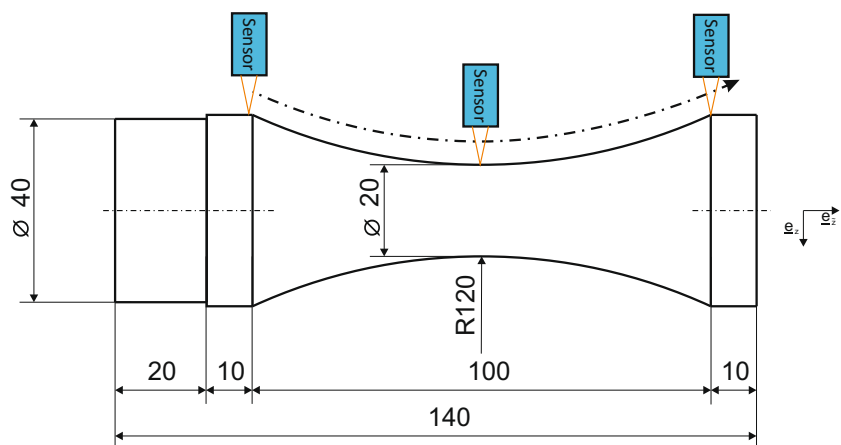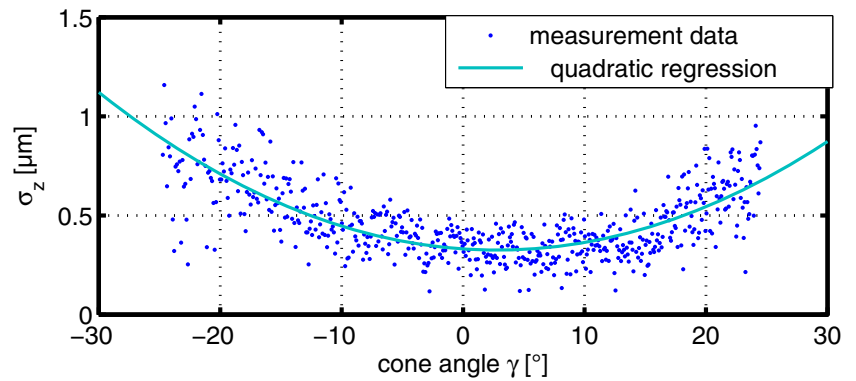
Fig. 8 Distance uncertainty versus cone angle γ. Each distance uncertainty is acquired from 100 consecutively measured distances at the rotating specimen depicted in Fig. 7. The regression indicates a quadratic increase of σ_z with increasing cone angle

measured first; the design drawing is depicted in Fig. 7. In Fig. 8, the corresponding distance standard deviations are presented. A steady increase of σ_z for an increasing $|\gamma|$ from $\sigma_z(\gamma = 0) = 0.28$ μm to $\sigma_z(|\gamma| = 25°) \approx 1$ μm is visible. A similar behavior is obtained for the relative velocity uncertainty increasing from 0.3 to 0.8 %. With $R = 20$ mm and $N = 100{,}000$, a standard deviation for the shape measurement of $\sigma_r = 1$ μm result for $|\gamma| = 25°$, cf. Eq. 9. Thus, the requirement for shape uncertainties below 1 μm are not fulfilled at highly tilted surfaces.

The increase in the shape uncertainty is due to two reasons, both resulting from measuring with the measurement axis $\underline{e}_z$ perpendicular to the rotational axis $\underline{e}_{\tilde{z}}$, which leads to a tilt between the surface normal and $\underline{e}_z$. On the one hand, the SNR decreases, since less scattered light is detected by the sensor (SNR$(\gamma = 0) = 10$ dB, SNR$(|\gamma| = 25°) = 0$ dB). The SNR decrease leads to an increase of the measurement uncertainty [27, 28]. On the other hand, the distance of the surface varies within the width w of the measurement volume. With $2w = 50$ μm, these distance variations amount up to $dz/d\tilde{z} \cdot w = \pm 10$ μm. Due to the speckle effect, the different distances are averaged with a random weighting factor.

Both the decrease in SNR as well as the increase in the distance variation for increasing γ can be resolved by measuring perpendicularly to the surface. This is possible in general for lathe monitoring, since the approximate macro geometry of the specimen is known a priori. We tested this approach for a measurement of a truncated cone with a cone angle $\gamma = 9°$. As a result, the standard deviation of the distance is reduced from $\sigma_z = 0.5$ to $\sigma_z = 0.28$ μm, as expected. If this approach is not feasible, because the sensor cannot be tilted, or if the approach is not wanted, the SNR can be increased, by increasing the laser power or numerical aperture and distance variation can be reduced by reducing $2w$.

Next to the cone angle, the influence of the mean radius R toward the achievable standard deviation is investigated. For this purpose, a step shaft with $R = 2.5, 5, 10, 20$ mm is

manufactured and measured. The measurement takes place at a constant rotational frequency of 25 Hz. The lateral resolution along the circumference of the specimen is set to a 1 mm, for comparability. Interestingly, neither $\sigma_z \approx 300$ nm nor $\sigma_v/v \approx 0.3$ % show any significant dependency toward R. This is important, since inserting $\sigma_v/v \approx 0.3$ % in Eq. 9 yields a constant relative uncertainty of the mean radius

$$\frac{\sigma_R}{R} = \frac{3 \cdot 10^{-3}}{\sqrt{N}}, \tag{10}$$

meaning that the measurement uncertainty for R decreases with decreasing R. Thus the σ_R decreases from about 200 nm for $R = 20$ mm down to about 25 nm for $R = 2.5$ mm. As a result, for small radii, the standard shape uncertainty is only limited by the standard deviation of the distance measurement. Furthermore, the independence of σ_r from v means, that the P-LDD sensor is well equipped for shape measurements at fast rotating surfaces, for instance in high speed cutting lathes.
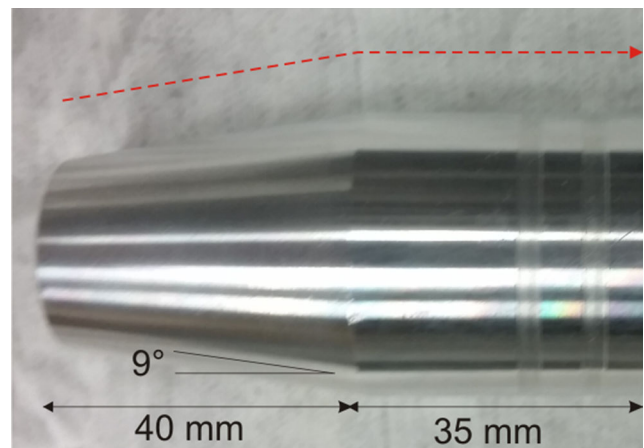

Fig. 9 Photograph of the workpiece. The traversing trajectory of the P-LDD sensor is marked by the *red dotted line*. Please note that the actual workpiece has a length of 100 mm; however, only the first 75 mm are depicted and are measured by the P-LDD sensor

Table 1 Comparison between in situ measurements and reference measurements

| Measurand	In situ	Reference
Mean diameter	37.9469 mm	37.9429 mm
Conic shape deviation	0.1 µm/mm	0.04 ± 0.05 µm/mm
2nd order deviation from circle	0.6 µm	0.3 to 0.8 µm
Groove spacing	100 µm	100 µm
Groove height	1.2 µm	1.1 µm

5 Three-dimensional shape measurements

Finally, the capabilities for in situ, absolute shape measurements of the P-LDD sensor are investigated. For this purpose, a workpiece is manufactured; the absolute shape of the workpiece is measured with the P-LDD sensor in situ and compared to ex situ measurements performed with a CMM for reference. The workpiece under test consists of a truncated cone ($\gamma = 9°$, length 40 mm), which is followed by a cylindrical profile ($R = 19$ mm, length 35 mm) with two circumferential notches (width 3 mm, depths 80 µm, and 200 µm). A photo of the workpiece is depicted in Fig. 9. The acquired measurement results are compared to the reference measurements in Table 1.

For the cutting process, the rotational frequency is set to 30 Hz and the feed velocity to 100 µm/revolution. For the measurements, the rotational frequency is set to 30 Hz

(as for the workpiece processing). The feed velocity for the measurement is set to 20 µm/revolution to achieve a dense data map along the height of the workpiece. With a total length of the workpiece of 75 mm, this results in a measurement time of 125 s and $N = 625,000$ data points. Since the maximum radius deviation of the workpiece at the truncated cone is larger than the length of the measurement volume, the P-LDD sensor is traversed along the $\tilde{z}\tilde{x}$-axis with a constant distance toward the surface of the workpiece at the cone, using a priori knowledge about the workpiece. At the cylindrical profile as well as at the notches, the sensor is transversed in $\tilde{z}$-direction only.

In Fig. 10, the measured velocity (top) and distance (bottom) are depicted. The conic expansion and cylindrical profile are clearly visible from the measured velocities, while the notches (and their convex profile, resulting from the cutting tool shape) become apparent from the distance measurement. For the distance measurement, a periodic oscillation is detected. Performing a frequency analysis shows that the oscillation frequency equals the rotational frequency and that the amplitude of the oscillation decreases from 10 µm at $\tilde{z} = 0$ to 3 µm at $\tilde{z} = 75$ mm. Furthermore, the oscillation frequency does not change when the feed velocity is changed. Decreasing f_{rot} reduces the oscillation amplitude however. This leads to the assumption that the oscillation originates from a tumbling of the workpiece due to axle play and is therefore disregarded for the shape measurement. Excluding the tumbling, a standard deviation

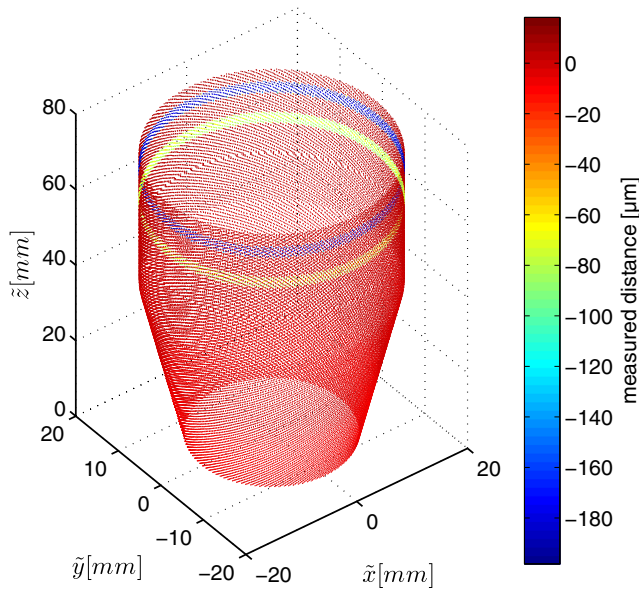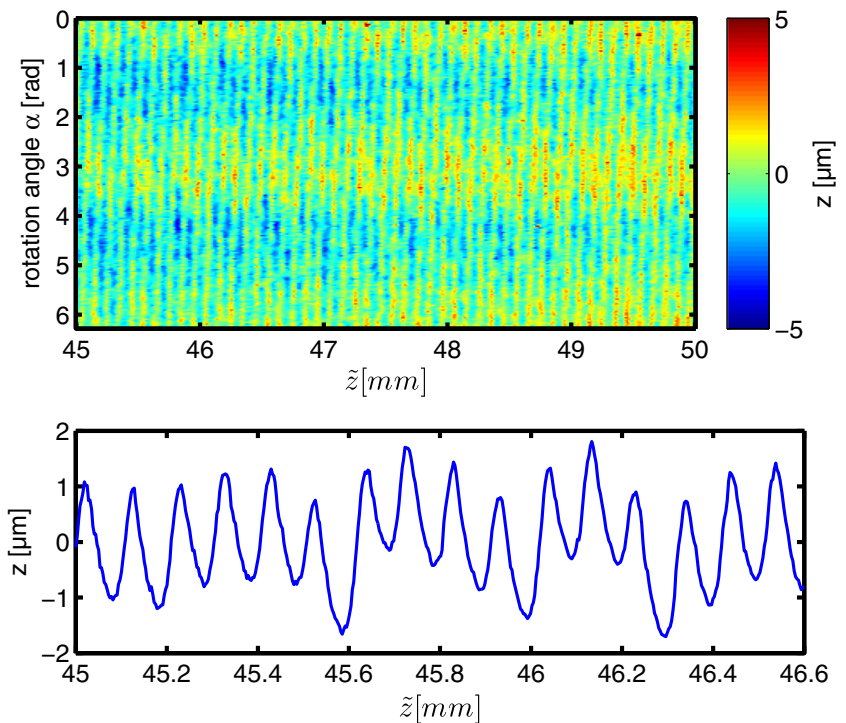**Fig. 10** Measured velocity v and distance z over the height $\tilde{z}$ of the workpiece
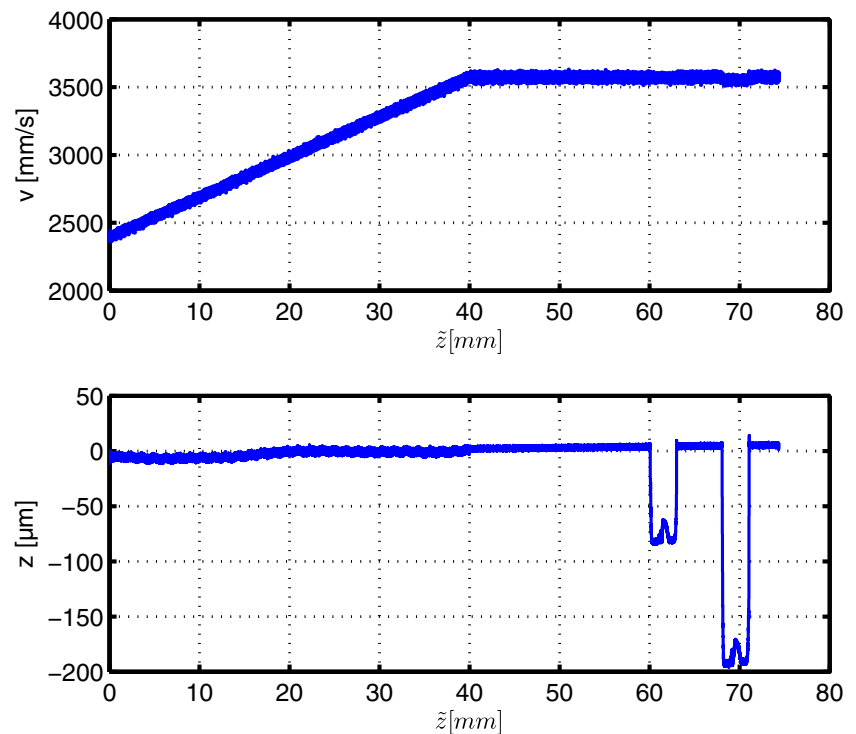
Fig. 11 Shape resulting from the v and z measurements. Color coding represents the measured distance and is used to highlight the measured notches

for the distance measurement of $\sigma_z = 0.28$ μm and a relative standard deviation for the velocity measurement of $\sigma_v/v = 0.3$ % is achieved again, as expected. The standard uncertainty for the in situ, absolute shape measurement $\sigma_r \approx 0.3$ μm results. By adding the traversing trajectory of the sensor to the measured distances, Eq. 5 the absolute shape of the workpiece results, which is depicted in Fig. 11.

This shows that the principle of an absolute shape measurement by a simultaneous velocity and distance measurement works. For reference of the absolute shape measurement, the mean diameter $D = 2R = 37.9469$ mm of the cylindrical part of the workpiece measured with the P-LDD sensor is compared to measurements with a CMM (ULM 600). For this purpose, two diameter measurements are performed in two planes (at $\tilde{z} = 54$ mm and at $\tilde{z} = 82$ mm) each, resulting in $D = 37.9429$ mm. Therefore, a total deviation for the mean diameter of 4 μm results. This is a factor of 2.5 larger than the combined standard uncertainty of both measurement systems, and needs further investigation in the future. One major influence not considered so far is the workpiece temperature, which was neither controlled nor measured. For the investigated workpiece (aluminum, $D \approx 40$ mm), a temperature difference of 1 K results in a diameter difference of nearly 1 μm. Thus, a temperature deviation of only 4 K would explain the observed measurement deviation. Therefore, the workpiece temperature during the in situ shape measurement is a major concern for first part quality manufacturing, especially in dry-machining. Ideally, the temperature should be controlled or at least measured and the resulting expansion of the workpiece modeled, respectively.

Next to the macro geometry, micro geometric shape deviations can be measured with the P-LDD sensor. In Fig. 12, the angle and height resolved distance is depicted for a segment of the cylindrical profile. Several deviations to a perfect cylinder become apparent. Firstly, a sinusoidal variation in the direction of the circumference with a mean

Fig. 12 *Top*: Measured surface profile with the P-LDD sensor, showing the ellipticity, grooves from the cutting tool and conic expansion of the workpiece. *Bottom*: Reference measurement performed with a nanofocus μsurf. Depicted is the mean roughness profile from a 1.6×1.6 mm^2 surface segment

amplitude of 0.6 μm is visible. This second-order deviation from a perfect a circle or ellipticity was confirmed by three shape measurement with a shapemeter MMQ3 F2P offering ellipticities of 0.3 to 0.8 μm.

Secondly, a conic expansion of the workpiece is visible along $\tilde{z}$. This expansion amounts to 0.1 μm/mm. A two-point reference measurement with the ULM 600 resulted in an expansion of 0.04 ± 0.05 μm/mm. Thus, the results are in good agreement.

Lastly, grooves with a spacing of 100 μm and a mean amplitude of 1.2 μm spiraling around the workpiece can be seen. Amplitude and spacing of the grooves are derived by a spatial frequency analysis of the measured surfaces profile. The grooves originate from the cutting tool, which was fed with 100 μm/revolution during the manufacturing of the workpiece. Reference measurements with a confocal microscope (nanofocus μsurf) at a segment show a 1.6×1.6 mm^2 surface segment very good agreement (mean groove amplitude 1.1 μm groove spacing 100 μm).

Concluding, the P-LDD sensor allows not only for a measurement of the mean diameter but also for measuring second (and even higher) order shape deviations from a perfect circle, conic expansions in the sub-micron range as well as grooves originating from the cutting tool.

6 Conclusion and outlook

A new approach for in situ 3D shape monitoring for lathes was presented. It is based on the evaluation of the axial position and the lateral velocity of the workpiece surface, making the shape measurement independent from the radial distance between sensor and surface. As optical sensor, the laser Doppler distance sensor with phase evaluation (P-LDD) allows the simultaneous measurement of both quantities and also offers keyhole access. The sensor allows high measurement rates of several kHz, since it requires only single point detectors and offers a velocity independent measurement uncertainty. The sensor was applied in a lathe for the first time and its performance regarding the surface roughness (micro-geometry), surface tilt as well as the workpiece diameter (macro-geometry) was investigated. The in situ measurements were compared to ex situ measurements with tactile coordinate measurement machines for reference.

A standard uncertainty of 0.3 μm for the absolute shape measurement inside of a lathe was achieved. Furthermore, the sensor enables an in situ measurement of grooves originating from deteriorated cutting tools as well as ellipticities and higher order shape deviations in the micron to sub-micron range. The measurement uncertainty of the shape results from the standard deviation of the position

measurement, which is below 300 nm, and from the relative standard deviation of the velocity measurement, which is 0.3 %. Both standard deviations are independent from the surface roughness for $R_a < 1$ μm and independent from the workpiece diameter. Increasing uncertainties at conic workpieces can be reduced by aligning the P-LDD sensor perpendicular to the workpiece surface employing a priori knowledge of the workpiece. Reference measurements with a tactile coordinate measurement machine show a deviation from the in situ measurements of 4 μm, which is assumed to be caused by temperature variations of the workpiece. These temperature variations have be to considered in the future, ideally by controlling or monitoring the workpiece temperature during the in situ shape measurement.

As an outlook, a more robust sensor head design with respect to thermal effects as well as an online signal processing are currently setup for industrial application. The online signal processing will provide the measurement data in real-time to allow a direct control of the production process. Furthermore, the influence of coolants on the surface towards the measurement uncertainty is to be investigated, in order to apply the sensor to near-dry machining as well. Lastly, the lateral resolution has to be improved to enable measurements at rotationally asymmetric workpieces.

References

1. Tönshoff HK, Arendt C, Amor RB (2000) CIRP Ann Manuf Technol 49(2):547
2. Zhang S, To S, Cheung C, Wang H (2012) Int J Mach Tool Manuf 62:1
3. Kim BS, Song YC, Park CH (2011) Int J Precis Eng Manuf 12(4):657
4. Inasaki I, Karpuschewski B, Tönshoff HK (2002). In: Sensors in Manufacturing, Volume 1 (Wiley-VCH Verlag GmbH), pp 203–235
5. Smith GC, Lee SS (2005) Int J Adv Manuf Technol 25(3–4):270
6. Jurkovic J, Korosec M, Kopac J (2005) Int J Mach Tools Manuf 45(9):1023
7. Zhang C, Zhang J (2013) Comput Ind 64(6):708

8. Ghani JA, Rizal M, Nuawi MZ, Ghazali MJ, Haron CHC (2011). In: Wear, 18 , vol 271, Philadelphia, USA, pp 2619–2624

9. Sata T, Takeuchi Y, Sakamoto M, Weck M (1981) CIRP Ann Manuf Technol 30(1):445

10. Han J, Wang L, Wang H, Cheng N (2012) Int J Adv Manuf Technol 62(1–4):205

11. Del Guerra M, Coelho RT (2006) J Mater Process Technol 179(1–3):117

12. Valio G, Surez C, Rico J, lvarez B, Blanco D (2012) Adv Mater Res 498:49

13. Andersson P, Hemming B (2015). In: Wear, vol 338–339, Toronto, Canada, pp 95–104

14. Chen F, Brown GM, Song M (2000) Opt Eng 39(1):10

15. Williams DC (2012) Optical methods in engineering metrology. Springer Science & Business Media, Dordrecht

16. Heist S, Mann A, Kühmstedt P, Schreiber P, Notni G (2014) Opt Eng 53(11):112208

17. Gräbler T, Drabarek P (2015). In: Proc. SPIE, vol 9525, Munich, Germany, pp 95,250O–95,250O–8

18. Matthias S, Kästner M, Reithmeier E (2015). In: Proc. SPIE, vol 9525, Munich, Germany, pp 952,513–952,513–8

19. Dreier F, Günther P, Pfister T, Czarske J, Fischer A (2013) IEEE Trans Instrum Meas 62(8):2297

20. Kuschmierz R, Filippatos A, Günther P, Langkamp A, Hufenbach W, Czarske J, Fischer A (2015) Mech Syst Signal Process 325:54–55

21. Günther P, Kuschmierz R, Pfister T, Czarske J (2012) Opt Lett 37(22):4702

22. Günther P, Kuschmierz R, Pfister T, Czarske J (2013) J Opt Soc Am A 30(5):825

23. Neumann M, Dreier F, Günther P, Wilke U, Fischer A, Bttner L, Holzinger F, Schiffer HP, Czarske J (2015) Mech Syst Signal Process 6465:337

24. Philipp K, Koukourakis N, Kuschmierz R, Leithold C, Fischer A, Czarske J (2015) Opt Lett 40(4):514

25. Truax BE, Demarest FC, Sommargren GE (1984) Appl Opt 23(1):67

26. Miles P, Witze PO (1996) Proc. 8th Int. Symposium an Application of Laser Techniques to Fluid Mechanics Lisabon/Portugal 40.1:1

27. Kuschmierz R, Czarske J, Fischer A (2014) Meas Sci Technol 25(8):085202

28. Pfister T, Fischer A, Czarske J (2011) Meas Sci Technol 22(5):055301 (15pp)

29. Kuschmierz R, Koukourakis N, Fischer A, Czarske J (2014) Opt Lett 39(19):5622